Fermi surface

October 10, 2019

Contents

1 Introduction / "Bold" Paragraph

Fascinations with strongly correlated electron systems continue, where key properties such as conductivity, magnetization sensitively depend on control parameters like temperature and applied electric or magnetic fields (refs to Natures). Tailoring of electronic states, in order to obtain "properties on demand" **?** is one of the main aims of modern theoretical physics.

Specifically, recent upheaval of interests in what happens when the system is put out of equilibrium, we can expect various novel phenomena which would be unthinkable in equlibrium situations. One promising direction is to apply time-dependent AC electric fields to correlated materials, which can lead to emergence of new states of matter, not only transiently but also as nonequilibrium steady states that retain their unusual properties long after the action of electric field.

The light-driven control of the many-body interaction has also been proposed in the Floquet formalism for the kinetic exchange interaction in the strong-coupling regime in ref. **?**. @HA also cite Kitamura @HA You have cited **?** below, so you need to say something about the work (a perturbation theory was also used to analyse ..., etc). @EG to be clarified by ME?

Now, one salient possibility is a "repulsion-attraction conversion", which has been proposed to occur when the Hubbard model, a typical model for electron correlation, is driven with an AC field (such as laser light)**?**. With the Floquet formalism, the one-electron band is inverted when the ac drive is sufficiently strong. The system then starts to have a nonequilibrium distribution, which is totally different from the equilibrium Fermi-Dirac distribution. Specifically, when we switch on the drive suddenly, we have an inverted population, or a "negative temperature". It can then be shown that a negative T for a Hubbard on-site interaction U is translated, via the density matrix, to a positive T with a Hubbard interaction inverted into $-U$. This implies that a nonequilibrium drive can put the repulsively interacting system into an attractively interacting one. This

was shown for a continuous ac drive, for which we can describe a system with Floquet theory that treats modulations periodic in time, which shows that the quantum states are changed into Floquet states (temporal analogue of the Bloch states). Tsuji et al went on to show that even a half-cycle pulse (or a monocycle pulse with asymmetric shapes) can achieve a repulsion-attraction conversion, where the physics is (a many-body version of) the π-pulse drive, i.e., a nonadiabatic shift ($\sim \pi$) of the population in momentum space.

These two approaches raise an interesting question: how does a crossover from the continuous-ac (Floquet) situation to the mono-cycle ($\sim \pi$-pulse) situation occur? In the present work we exactly address this quetion. For drive forms that interpolate from a mono-cycle to continuous waves, we have calculated the total energy and the double occupancy, which are measures of the effective interaction, for the repulsive Hubbard model. This was done for various values of the repulsive interaction U, and various amplitude, frequency and pulse width of the ac drive.

It is now well recognized that correlated systems can have long-lived non-thermal states that do not relax to the thermal ones after the driving field is switched off **?**.? Thus rearrangements of electronic structure and distribution during and after the drive can indeed bring the system into the states inaccessible via adiabatic or thermal pathways**?**.

In the recent time significant @HA experimental? @EG to be clarified by MIK?

efforts have been done in this direction, e.g., selective pumping of phonons **?**, ... As it was shown in Ref. **??** the intraband transitions can play a crucial role in the optical response during the light-matter interaction in case of semiconductors.

Due to electronic nature of this mechanism, not including electron-phonon interaction, the characteristic time of phase change could be as fast as few fs. @HA what do you want to imply by this statement?. @EG that the mechanism doesn't necessarily includes phonons, so respond time can be very low

Transient superconductivity **?**.?

Time-dependent DOS and quantum oscillations, exact diagonalization for lattice model, Fermi-arc metal**?**.

Dynamics of Hubbard Model **????**. @HA cite Sayyad @EG we added references, which are still missing?

A nontrivial current generation by ultrashort laser pulse in the 2d system (graphene) and it's dependence on the phase matching condition of the pulse was described recently **?**.?

In the present paper we address three (?) main topics:

(i) Intense laser pulse induce dynamical localization in the correlated lattice, and during this process the HHG process takes place. The system behavior during the pulse and details of the phase transition are described in Sec. **??**.

(ii) Intense laser pulse brings correlated system to a different state, that could not be accessed adiabatically. These states are non-thermal and long-lived. The details of these states, as well as transient dynamics are described in Sec. **??**.

(iii) During the laser pulse, despite high field intensity and completely out-of-equilibrium state of the system, such concepts as Fermi surface (FS), Hubbard bands, quasiparticle peak still have the physical meaning and can be evaluated numerically. Details of the Fermi surface properties are discussed in Sec. **??**.

The organization of the present paper is as follows: @HA @EG Structure will be clarified later For the calculation we adopt the dynamical mean-field theory (DMFT), where we employ the nonequilibrium iterated perturbation theory (IPT). This is presented in Section 2. The benchmark of our method against the exact diagonalization technique in Ref.**?** is presented in Sec. **??**.

2 Model and method

We take the single-band Hubbard model driven by an electric field with the Hamiltonian,

$$H(t) = \sum_{ij,\sigma} t_{ij} \exp\left(-i \int_{\mathbf{R}_j}^{\mathbf{R}_i} d\mathbf{r} \cdot \mathbf{A}(t)\right) c^\dagger_{i\sigma} c_{j\sigma} + U \sum_i \left(n_{i\uparrow} - \frac{1}{2}\right)\left(n_{i\downarrow} - \frac{1}{2}\right), \tag{1}$$

where t_{ij} are electron hopping amplitudes between sites i and j, U is the on-site Coulomb interaction, $c^\dagger_{i\sigma}$ creates an electron at site i and spin σ, and $n_{i\sigma} = c^\dagger_{i\sigma} c_{i\sigma}$ is the number operator. We incorporate the effect of an external electric field $\mathbf{F}(\mathbf{t}) = -\partial \mathbf{A}(t)/\partial t$ in terms of the Peierls substitution for the vector potential $\mathbf{A}$ into the hopping**?** **?**. We assume the band is half-filled.

Here we take the two-dimensional square lattice having non-equivalent spatial directions.

The wave vector of pump pulse electromagnetic field is perpendicular to the plane of the two-dimensional lattice.

Exploiting this property we can direct electric field along one of the crystallographic axes, which gives a quasi one-dimensional model, or along the diagonal of the square lattice which gives physics similar to the one in Bethe or hypercubic lattices but with the two-dimensional band structure that includes the van Hove singularity and sharp band edges.

In order to treat the time-dependent problem, we use non-equilibrium extension of DMFT **??**, the realization of the algorithm is described in ref. **?**. We work within the Keldysh formalism (cite), adopting ... code (cite Martin!!) As an impurity solver we use the iterated perturbation theory (IPT) method, the expansion is performed in powers of interaction.

We consider the square lattice with the band dispersion,

$$\varepsilon(\mathbf{k}, t) = 2t\left[\cos(k_x + A_x(t)) + \cos(k_y + A_y(t))\right] + 4t' \cos(k_x + A_x(t)) \cos(k_y + A_y(t)), \tag{2}$$

where $t(t')$ is the nearest-neighbor (second-neighbor) hopping amplitude.

For the second part of the paper looking into material-specific Fermi surfaces in Sec. **??**, we use a tight-binding model for $YBa_2Cu_3O_y$ (YBCO) with $t = 0.69$ eV, $t' = -0.22$ eV, adopted from Ref. **?**. We ignore hoppings farther than the second neighbor, since the essential features, e.g. Fermi surface topology, are already captured by this model.

The quantities we have calculated are the following:

the kinetic energy,

$$E_{\text{kin}}(t) = -i \sum_{\mathbf{k}} \varepsilon_{\mathbf{k}} G^<_{\mathbf{k}+\mathbf{A}(t)}(t, t), \tag{3}$$

where $\tilde{G}^<_{\mathbf{k}}(t, t)$ is the gauge-invariant **?** lesser Green function in the Keldysh formalism.

The potential energy,

$$E_{\text{pot}}(t) = U\left\langle \left(n_\uparrow - \tfrac{1}{2}\right)\left(n_\downarrow - \tfrac{1}{2}\right)\right\rangle = U[d(t) - \tfrac{1}{2}(n_\uparrow + n_\downarrow) + \tfrac{1}{4}], \tag{4}$$

where $n_\sigma = c^\dagger_\sigma c_\sigma$ is a fermionic number operator, and $d(t) = \langle n_\uparrow(t) n_\downarrow(t)\rangle$ denotes the time-dependent double occupancy.

The total energy,

$$E_{\text{tot}}(t) = E_{\text{kin}}(t) + E_{\text{pot}}(t). \tag{5}$$

The electron momentum distribution function defined by

$$f(\mathbf{k},t) = -i\tilde{G}^{<}_{\mathbf{k}}(t,t) = -iG^{<}_{\mathbf{k}+\mathbf{A}(t)}(t,t). \tag{6}$$

The population density is calculated as

$$G^{<}(\omega,t) = -\frac{1}{\pi}\mathrm{Im}\int ds e^{i\omega s}G^{<}(t,t-s), \tag{7}$$

Current operator is defined as

$$\mathbf{j}(t) = -\frac{ie}{V}\sum_{\mathbf{k}\sigma} v_{\mathbf{k}}G^{<}_{\mathbf{k},\sigma}(t,t), \tag{8}$$

where V is the volume, e - charge of electron (equal to 1 in our units).

Now we describe the nonequilibrium drive. The electric field is given as

$$E(t) = -\partial\mathbf{A}(t)/\partial t \tag{9}$$

in terms of the vector potential $\mathbf{A}(t)$. As mentioned above, the crossover from monocycle to continuous-wave situations are considered for four types of the parameter changes of the laser pulse:

(i) frequency change of monocycle pulse,

(ii) transition from monocycle, high-frequency pulse to multicycle high-frequency pulse,

(iii) transition from monocycle low-frequency pulse to multicycle high-frequency pulse with the same pulse width (FWHM), and

(iv) transition from monocycle low-frequency pulse to multicycle low-frequency pulse (see Fig.**??**). For this purpose we define the time-dependent vector potential,

$$A(t) = A_{\max}\exp\left[-\frac{(t-t_0)^2}{2\sigma^2}\right] sin(\omega(t-t_0)), \tag{10}$$

where parameters are:

$\sigma = \frac{d}{2\sqrt{2ln2}}$: pulse duration with d: full-width at half-maximum (FWHM),

$A_{\max}$: amplitude of the vector potential,

ω: frequency of the vector potential,

t_0: peak time of the pulse.

3 Square lattice

3.1 Selection of the parameters for the construction of the Fermi surfaces

In calculating the Fermi surface, it is necessary to move away from considering local quantities to k-resolved. In the first part of the work, we will consider a square lattice with the nearest neighbors by hopping. Using the Green's functions on the Keldysh contur for a finite-dimensional lattice is computationally expensive and limits the time of simulations. Thus, in this chapter, we focus on transient dynamics and states immediately after the pulse. Therefore, we determine the system parameters at which the Fermi surface interpretation will be the best.

In the presence of a partical-hall symmetry, the challenge is to achieve a decay of the Green's functions during consideted simulation time. In the case of local Green's functions, the damping occurs rather quickly for various polarizations of the external

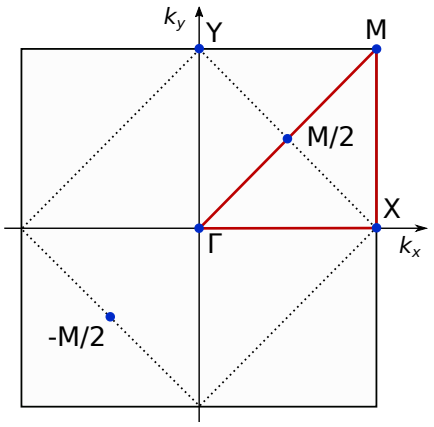

Figure 1: Brillouin zone for a square lattice.

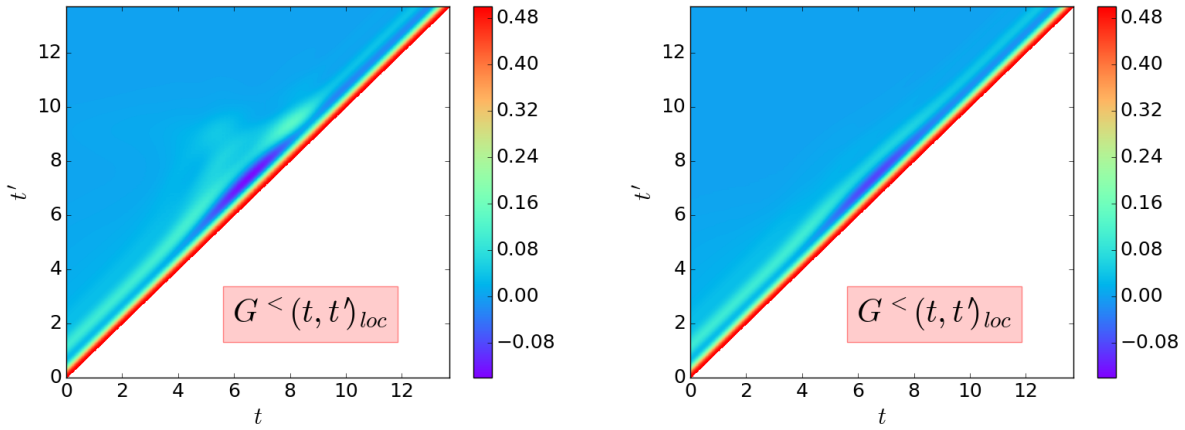

Figure 2: Local $G^<(t,t')$ for A=1.75 and U=6 with different polarizations of vector potential: (a) XY- polarization; (b) Y-polarization.

field 2. Such attenuation in time will give a quantitatively correct result in the Fourier transform to the frequency dependence quantities.

In the case of k-resolved Green's Functions, the damping is much slower for some k-points. In Figure 3 the dependence of the Green Function on time for different U is shown for Y and M/2-points in Brulluen zone. With increasing Coulomb interaction, the dumping of the Green Function is stronger. These highly symmetrical points were chosen due to the fact that they have the highest intensity of the spectral function at a frequency equal to zero and the smallest attenuation of the corresponding two-time Green's function.

In Figure 4 is shown the dependence of the Green Function on time for different value of vector potential for XY-polarization of vector potential. An increase in the vector potential leads to a faster decay of the Green's function.

The corresponding spectral functions are shown in the Figure 5. Some of them have negative values [Turkowski and Freericks, 2005, 2006, Freericks and Turkowski, 2009, Shen et al., 2014] that partially appear as a result of the selected Fourier transform.

As can be seen from the Figures 6 of the Green Functions versus time for the y-polarization of the field, a similar dependence of the attenuation on the magnitude of the vector potential.

Also, by analogy with the vector potential in diagonal direction, Y-direction transfers states Figure7a and particles Figure 7b from the low-frequency region to the high-frequency.

To understand how the redistribution of electrons occurs due to increasing of the

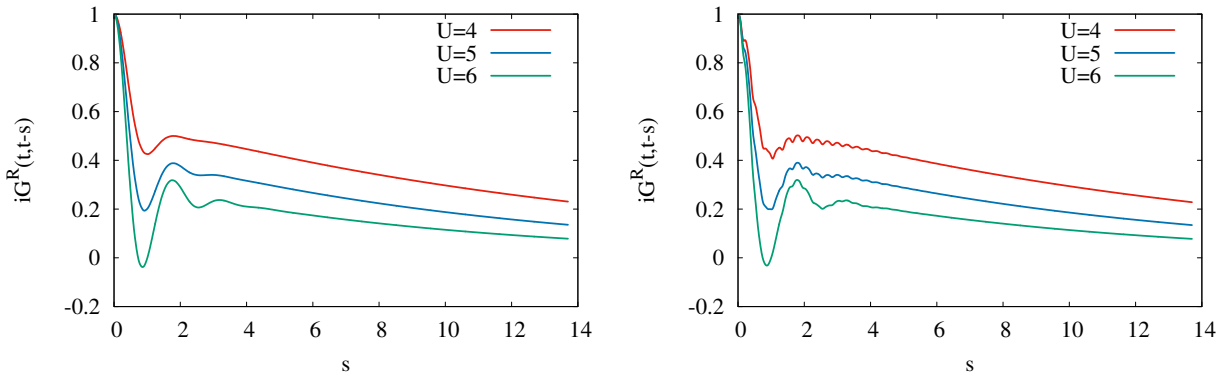

(a) (b)

Figure 3: $G^R(t, t-s)_k$ (t=6.85) with different U values for A_{max}=1.5 and XY-polarization: (a) Y-point of BZ; (b) M/2-point of BZ.

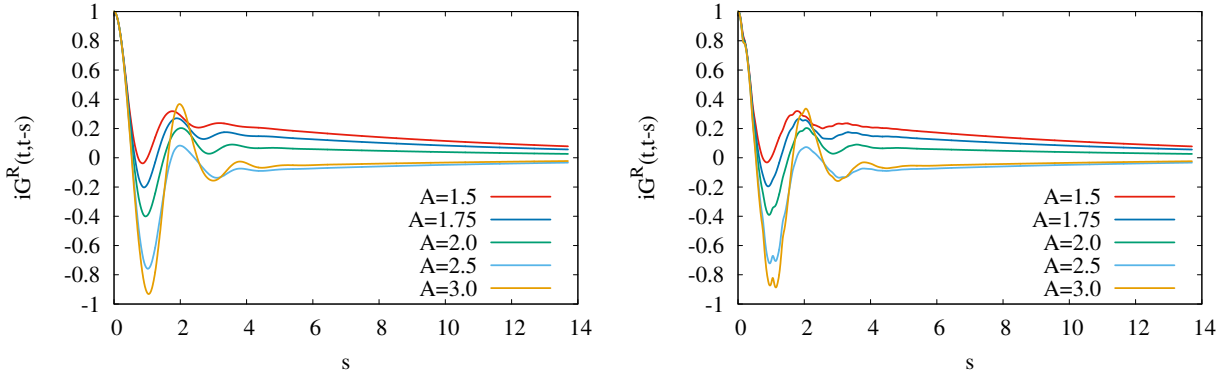

(a) (b)

Figure 4: $G^R(t, t-s)_k$ (t=6.85) with different A_{max} values for U=6 and XY-polarization : (a) Y-point of BZ; (b) M/2-point of BZ.

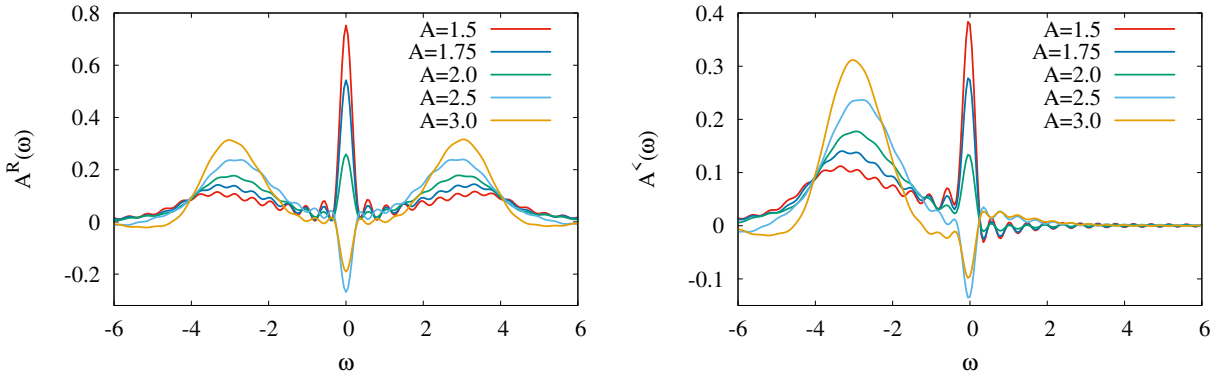

(a) (b)

Figure 5: Spectr of full number of states $G^R(t = 6.85, \omega)_k$ (a) and occupied states $G^<(t = 6.85, \omega)_k$ (b) with different A_{max} values for U=6 and XY-polarization in Y-point of BZ.

magnitude and direction of the pulse, we consider the local lesser Green Functions (Figure 8). For all directions of the pulse, the maximum pumping of the Hubbard bands occurs in the region of the middle of the pulse (t=6.85) due to the transfer of electrons to higher energy of the order of $U/2$. The higher the value of the vector potential, the stronger the intensity of the Hubbard zone and less in the low-frequency region for the Y-direction

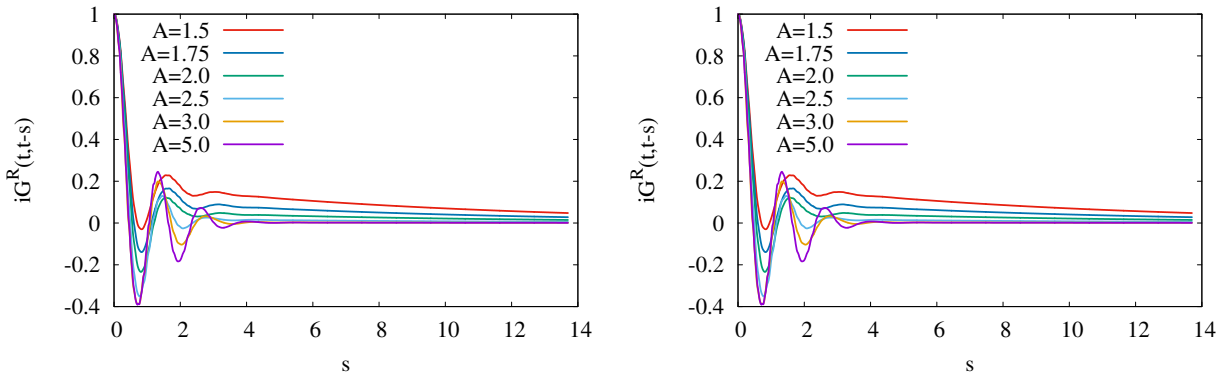

(a) (b)

Figure 6: $G^R(t, t-s)_k$ (t=6.85) with different A_{max} values for U=6 and Y-polarization: (a) Y-point of BZ; (b) M/2-point of BZ.

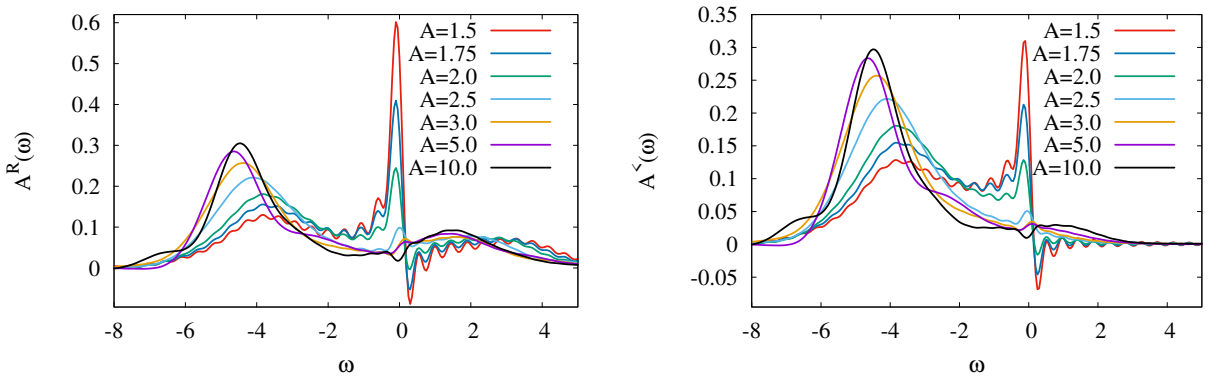

(a) (b)

Figure 7: Spectr of full number of states $G^R(t = 6.85, \omega)_k$ (a) and occupied states $G^<(t = 6.85, \omega)_k$ (b) with different A_{max} values for U=6 and Y-polarization in Y-point of BZ.

of the vector potential (Figures 8b,d,f). In the case of a diagonal pulse direction, the filling of the Hubbard band can oscillate depending on the renormalized hopping value in accordance with the zero order Bessel function.

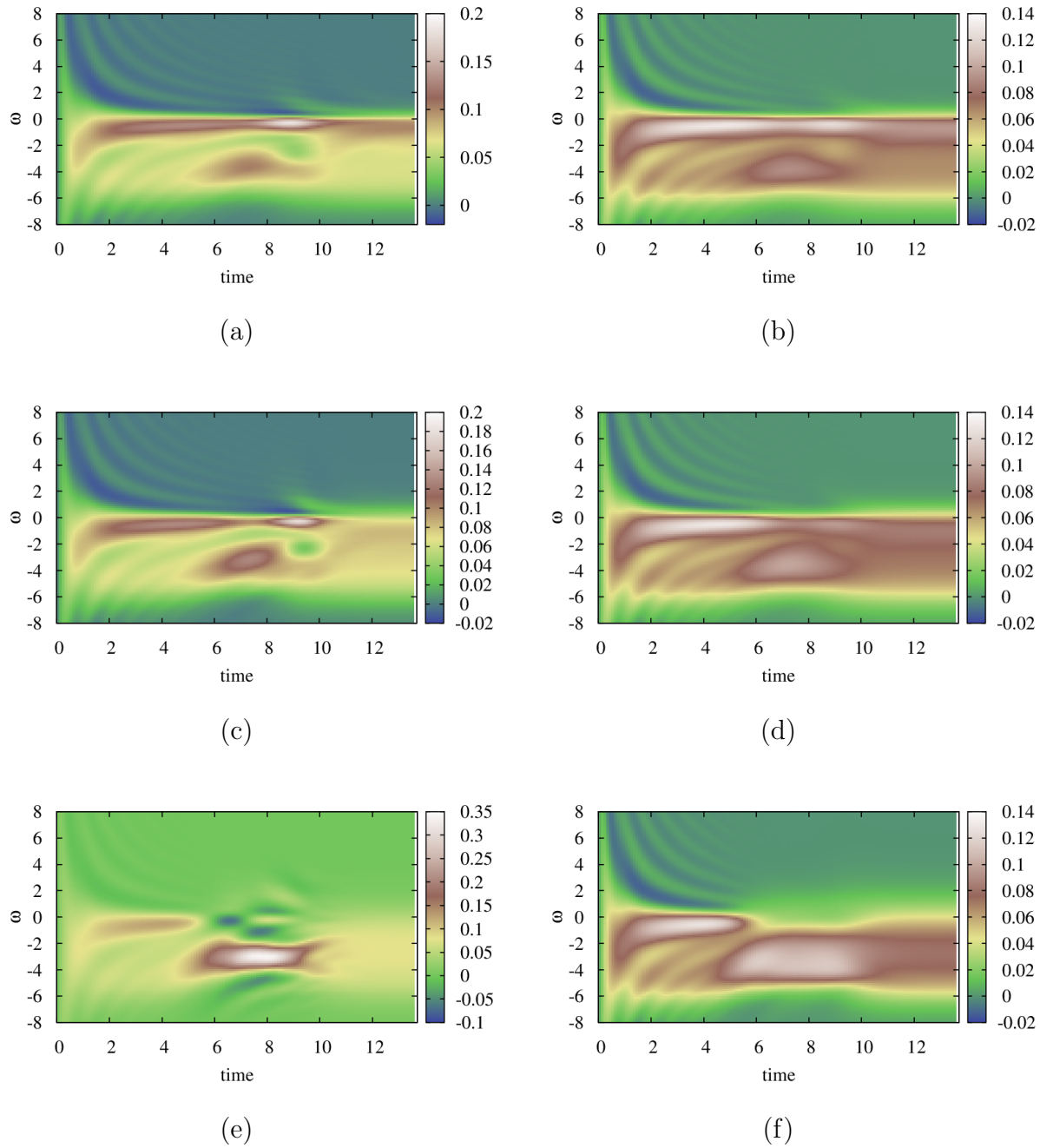

Figure 8: Occupied states $G^{<}(t,\omega)$ for U=6: (a) A_{max}=1.5 XY-polarization; (b) A_{max}=1.5 Y-polarization; (c) A_{max}=1.75 XY-polarization; (d) A_{max}=1.75 Y-polarization; (e) A_{max}=3.0 XY-polarization; (f) A_{max}=3.0 Y-polarization.

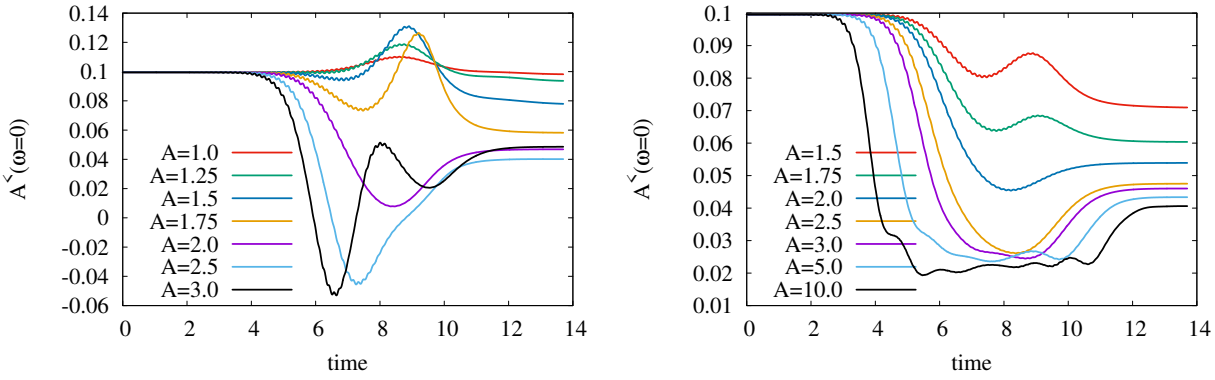

(a) (b)

Figure 9: (a) XY; (b) Y. U=6.

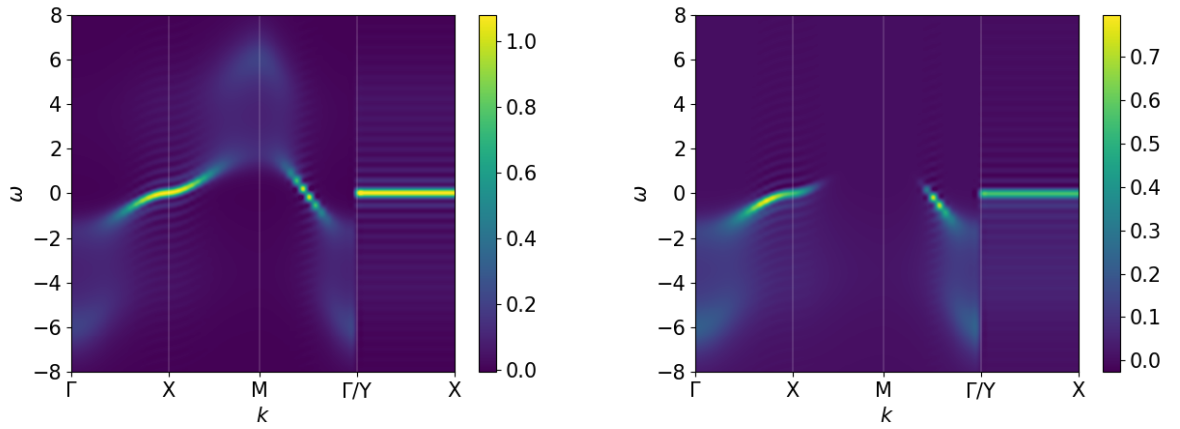

(a) (b)

Figure 10: Equilibrium (a) Band; (b) OCC. U=6.

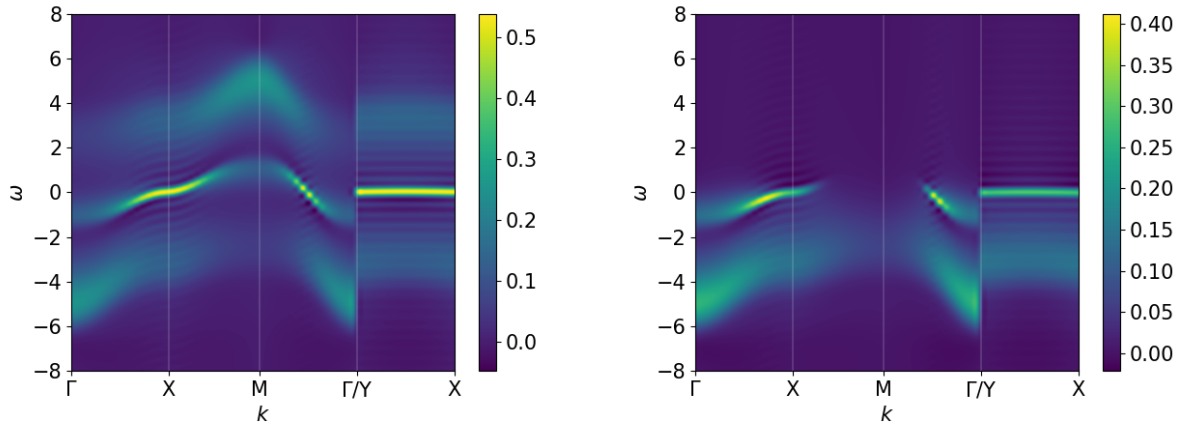

(a) (b)

Figure 11: A=1.75 (a) Band; (b) OCC. U=6. xy.

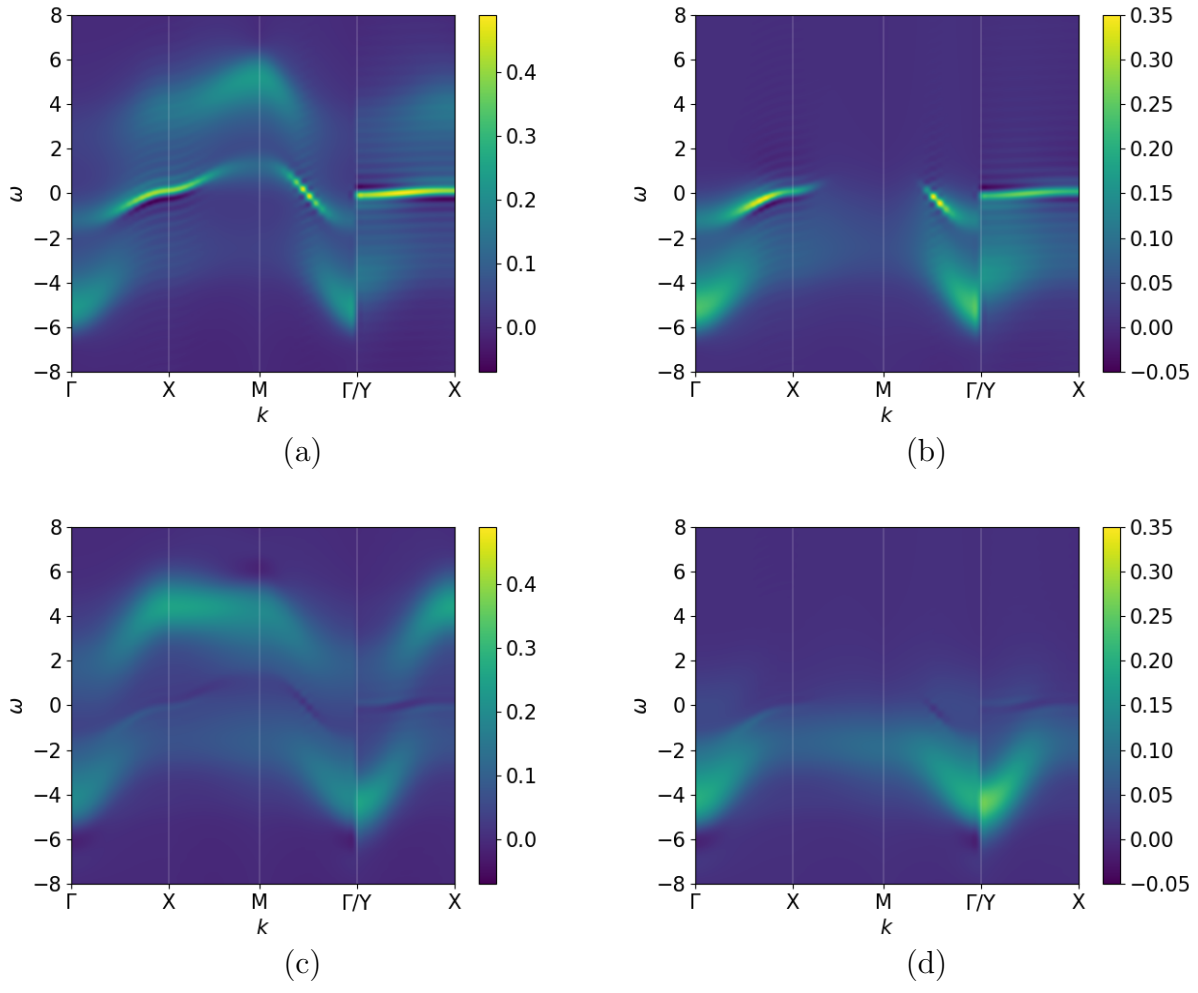

Figure 12: (a) band A=1.75; (b) OCC A=1.75; (c) band A=3.0; (d) OCC A=3.0; U=6. y.

3.2 Time dependent Fermi surface

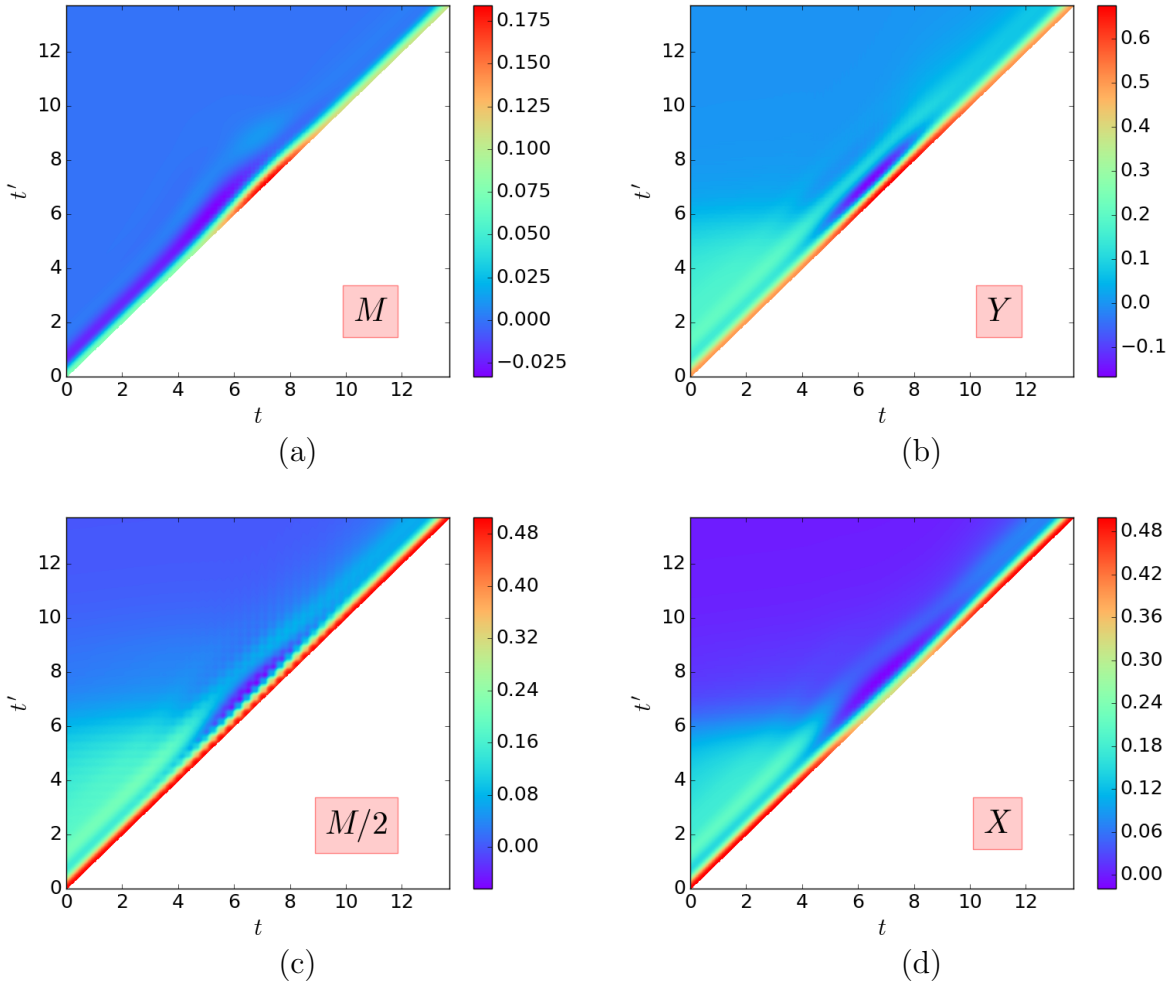

Figure 13: A=1.75: (a) M; (b) Y; (c) M/2; (d) X. y.

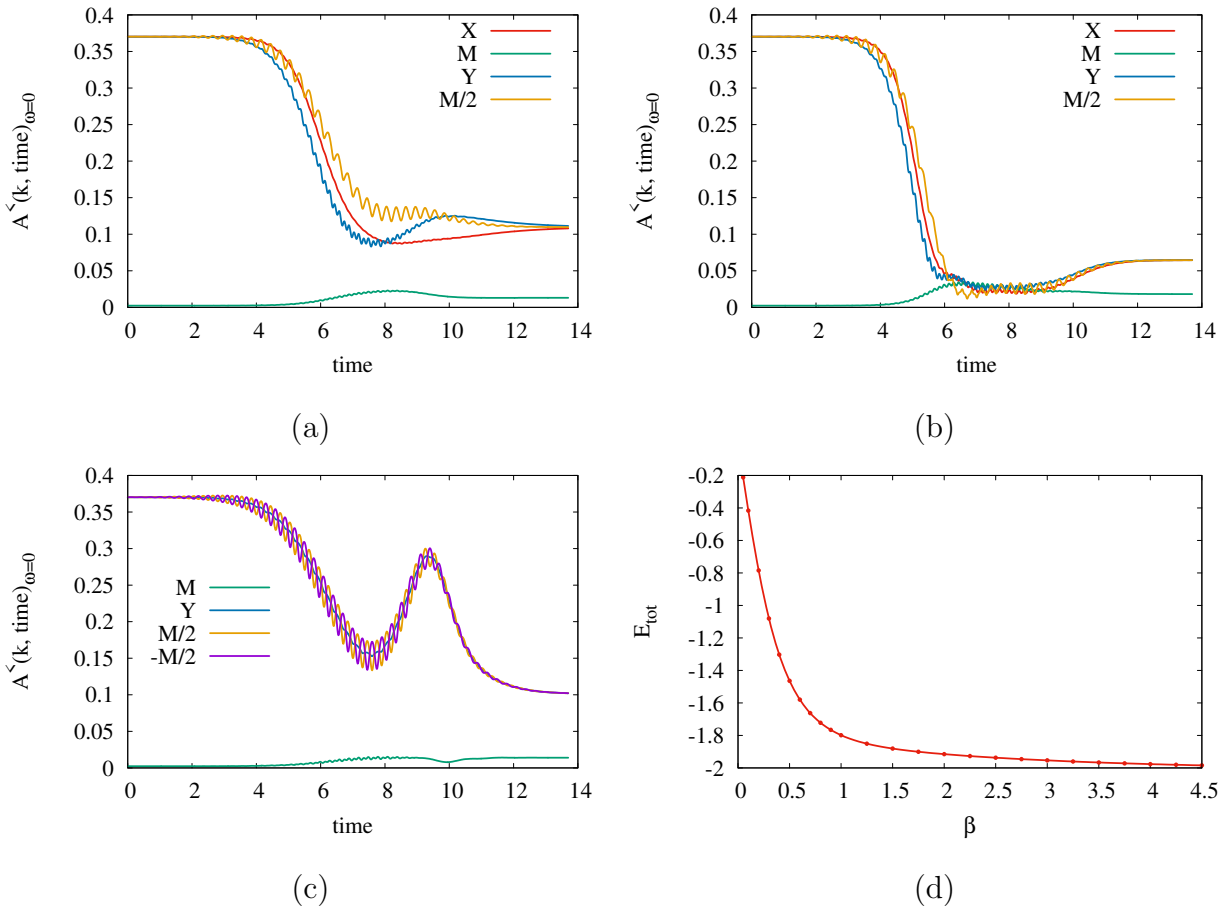

Figure 14: (a) A=1.75 y; (b) A=3.0 y; (c) A=1.75 xy; (d) temperature.

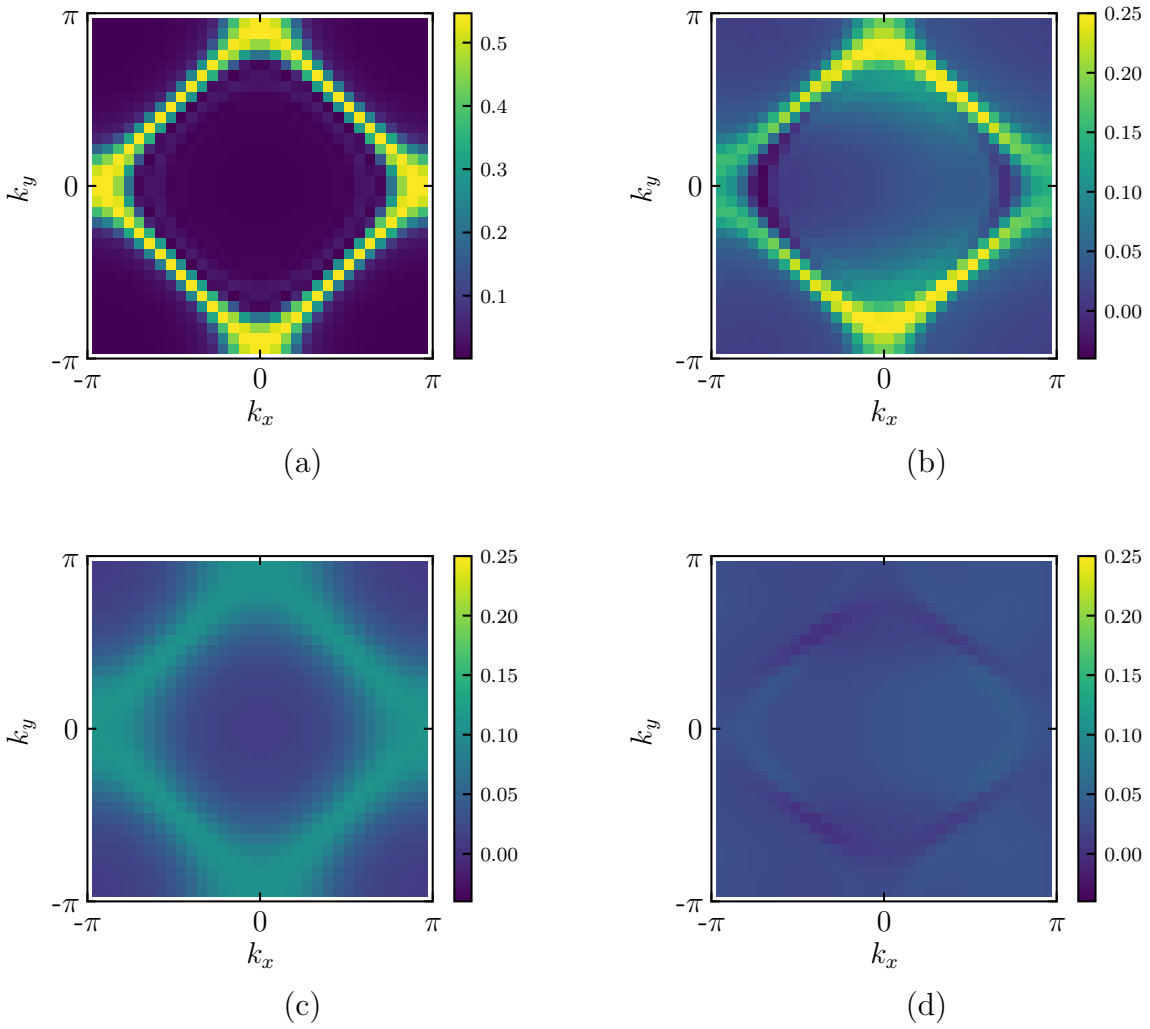

Figure 15: FS y-field: (a) equilibrium; (b) A=1.75 mid pulse; (c) A=1.75 after pulse; (d) A=3.0 mid pulse.

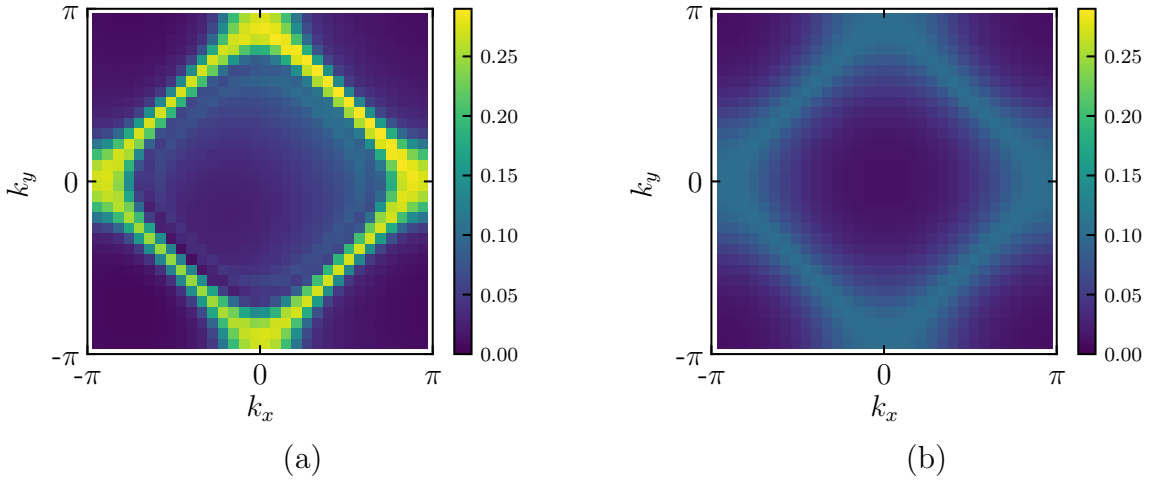

Figure 16: FS xy-field A=1.75: (a) mid pulse; (b) after pulse.

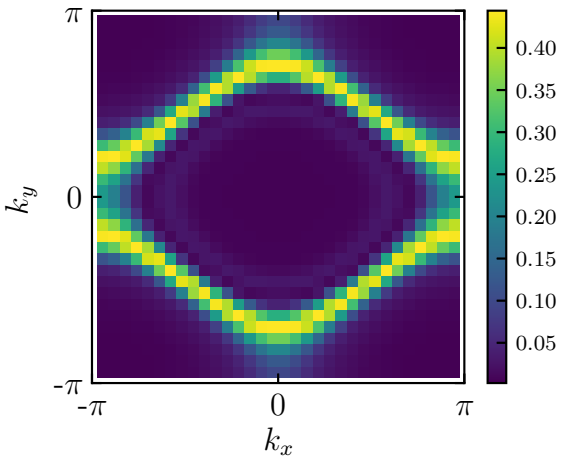

Figure 17: Steady state. for A=1.75, Y-field, beta=5, n=0.425

4 t-t' lattice

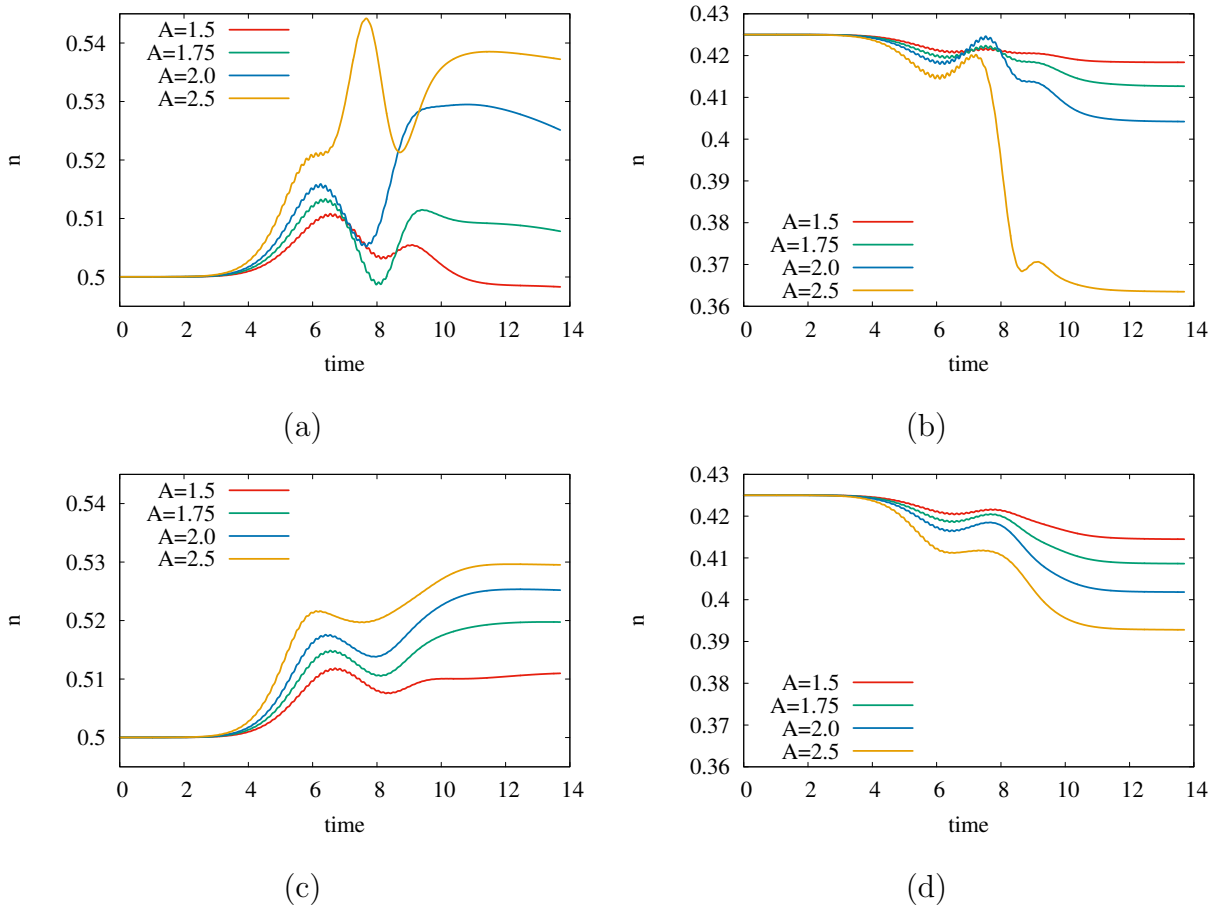

Figure 18: Particle Conservation: (a) n=0.5 xy; (b) n=0.425 xy; (c) n=0.5 y; (d) n=0.425 y.

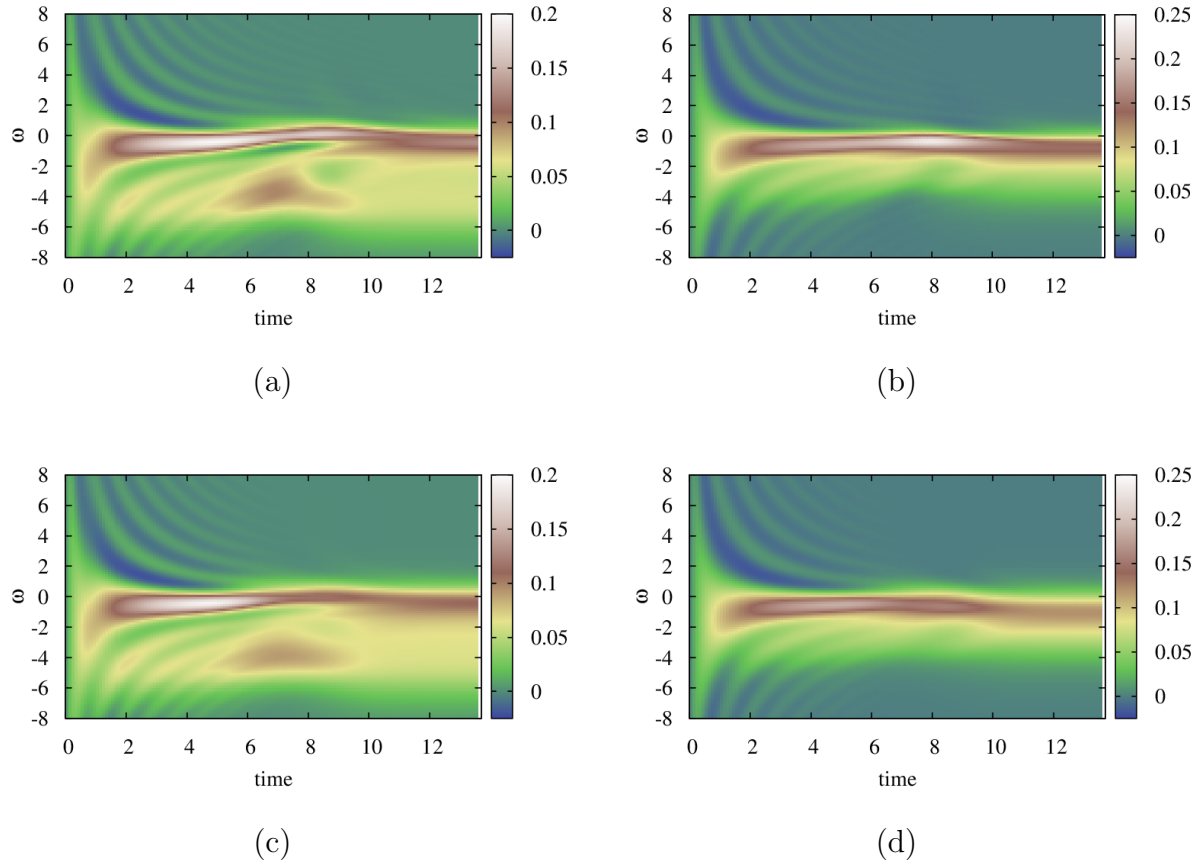

Figure 19: DOS A=1.75: (a) n=0.5 xy; (b) n=0.425 xy; (c) n=0.5 y; (d) n=0.425 y

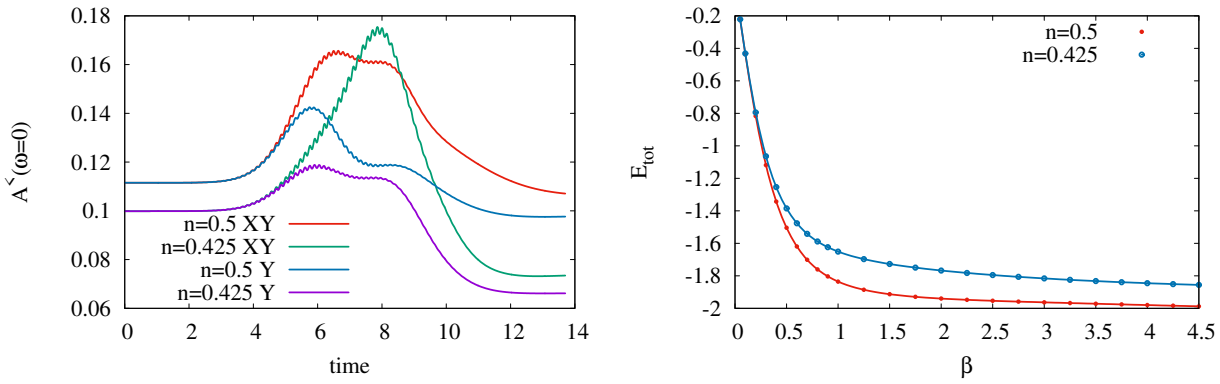

Figure 20: A=1.75: (a) A(w=0); (b) temperature.

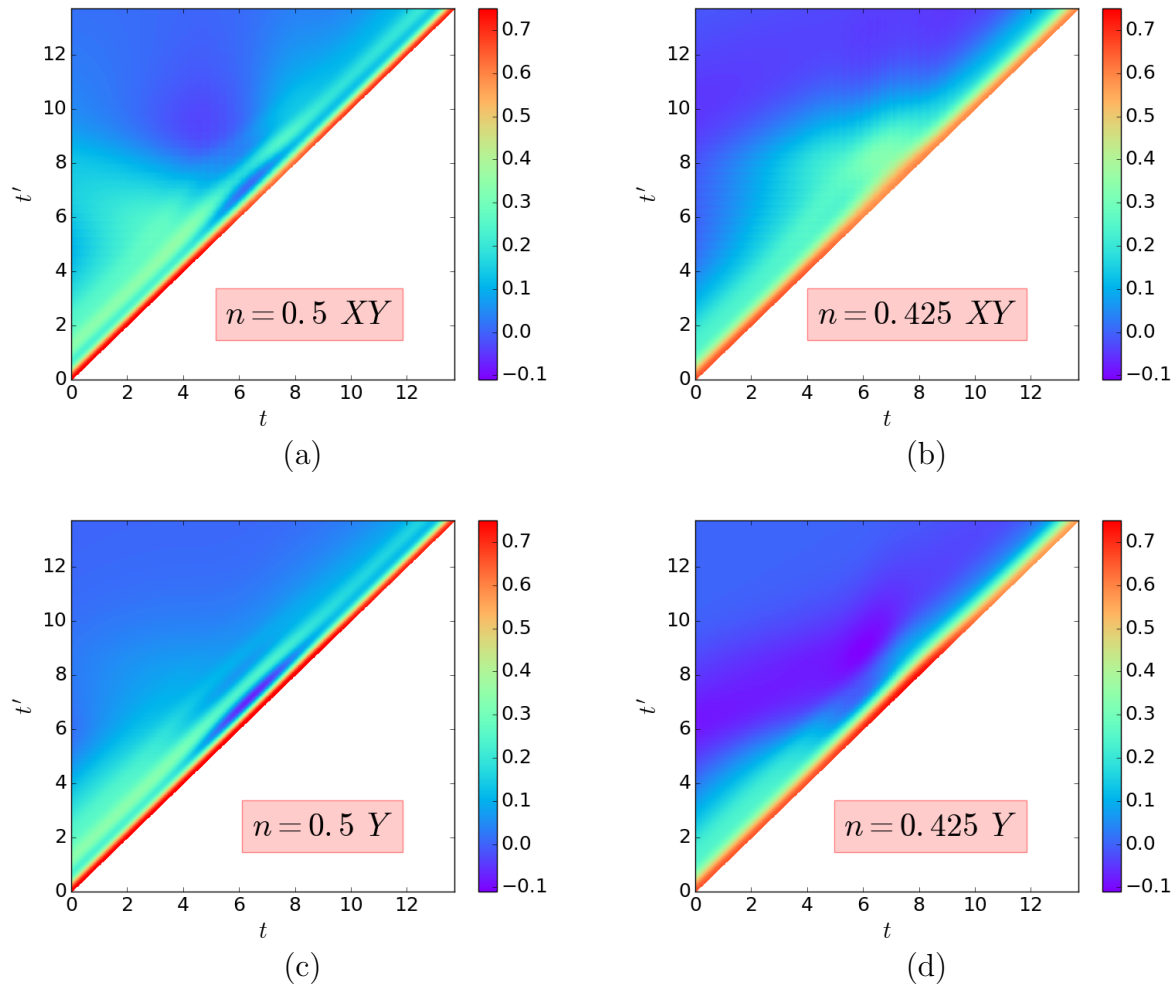

Figure 21: G les Y point A=1.75: (a) n=0.5 xy; (b) n=0.425 xy; (c) n=0.5 y; (d) n=0.425 y

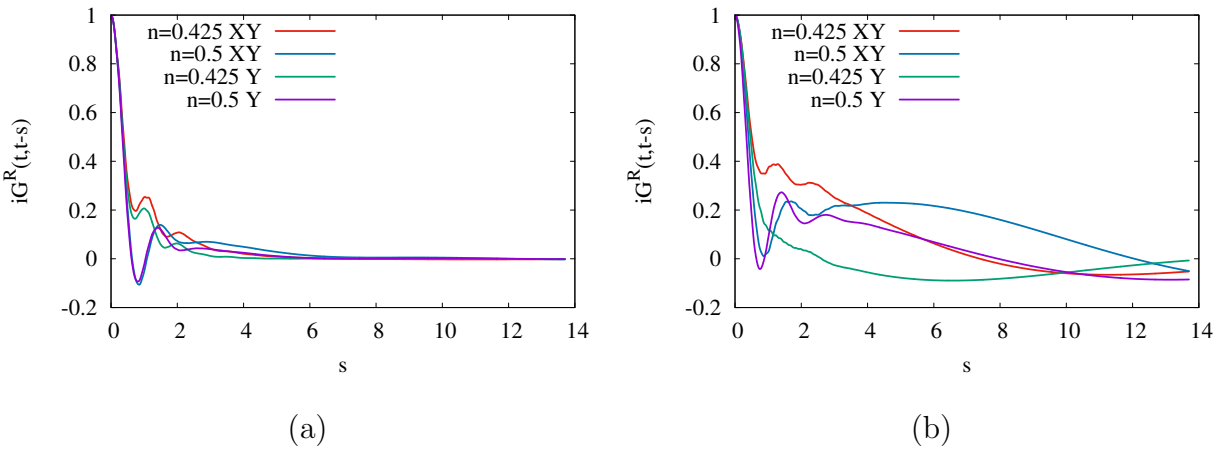

Figure 22: Gret A=1.75: (a) loc; (b) Y point.

4.1 Time dependent Fermi surface t-t'

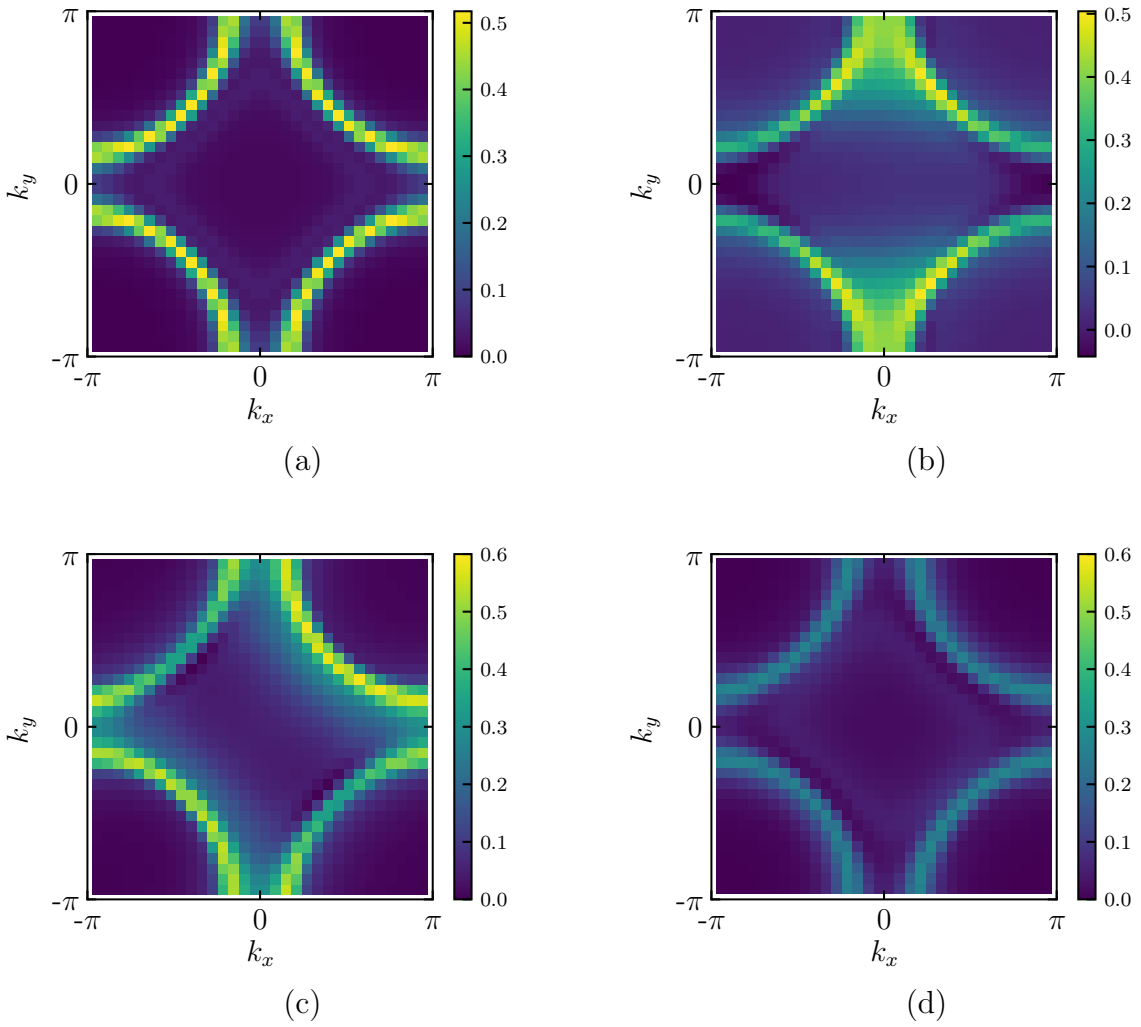

Figure 23: FS A=1.75: (a) equilibrium; (b) Y-field mid pulse; (c) XY-field mid pulse; (d) XY-field end pulse.

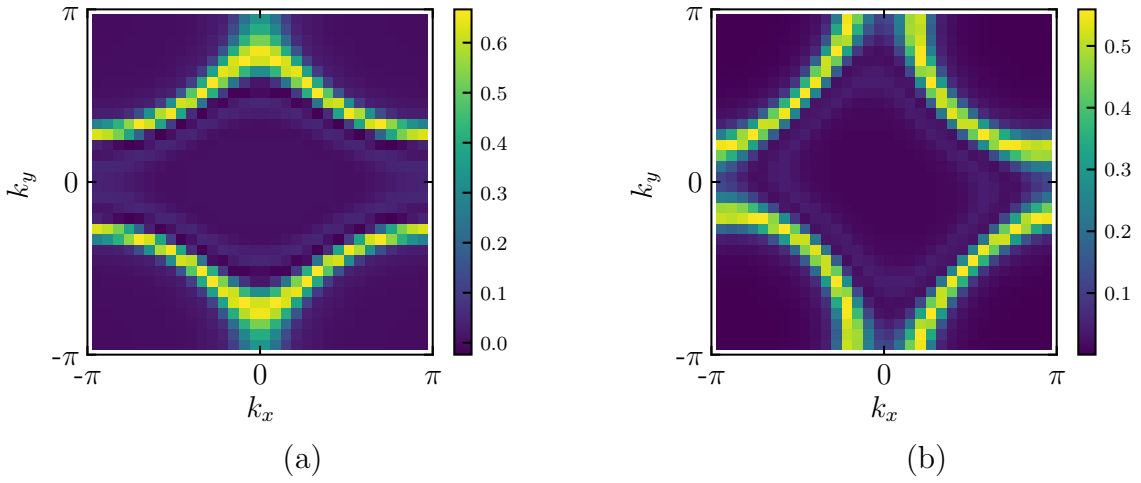

Figure 24: FS A=1.75 n=0.425 steady-state: (a) Y-field; (b) XY-field.

References

J. K. Freericks and V. Turkowski. Inhomogeneous spectral moment sum rules for the retarded green function and self-energy of strongly correlated electrons or ultracold fermionic atoms in optical lattices. *Phys. Rev. B*, 80:115119, Sep 2009. doi: 10.1103/PhysRevB.80.115119. URL https://link.aps.org/doi/10.1103/PhysRevB.80.115119.

W. Shen, Y. Ge, A. Y. Liu, H. R. Krishnamurthy, T. P. Devereaux, and J. K. Freericks. Nonequilibrium "melting" of a charge density wave insulator via an ultrafast laser pulse. *Phys. Rev. Lett.*, 112:176404, May 2014. doi: 10.1103/PhysRevLett.112.176404. URL https://link.aps.org/doi/10.1103/PhysRevLett.112.176404.

V. Turkowski and J. K. Freericks. Nonlinear response of bloch electrons in infinite dimensions. *Phys. Rev. B*, 71:085104, Feb 2005. doi: 10.1103/PhysRevB.71.085104. URL https://link.aps.org/doi/10.1103/PhysRevB.71.085104.

V. M. Turkowski and J. K. Freericks. Erratum: Spectral moment sum rules for strongly correlated electrons in time-dependent electric fields [phys. rev. b 73, 075108 (2006)]. *Phys. Rev. B*, 73:209902, May 2006. doi: 10.1103/PhysRevB.73.209902. URL https://link.aps.org/doi/10.1103/PhysRevB.73.209902.